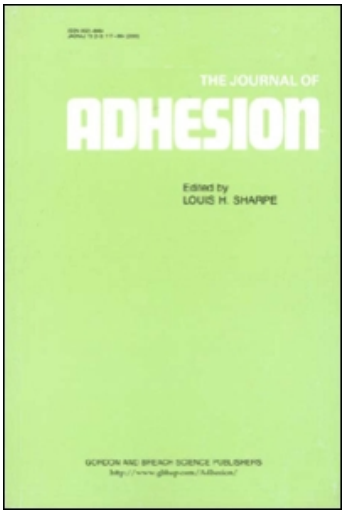

The Journal of Adhesion
Publication details, including instructions for authors and subscription information:
http://www.informaworld.com/smpp/title~content=t713453635

Peel Adhesion: Influence of Surface Energies and Adhesive Rheology

D. H. Kaelble[a]
[a] Central Research Laboratories, 3M Co., St. Paul, Minn.

To cite this Article Kaelble, D. H.(1969) 'Peel Adhesion: Influence of Surface Energies and Adhesive Rheology', The Journal of Adhesion, 1: 2, 102 — 123
To link to this Article: DOI: 10.1080/00218466908078882
URL: http://dx.doi.org/10.1080/00218466908078882

Peel Adhesion: Influence of Surface Energies and Adhesive Rheology

D. H. KAELBLE

Central Research Laboratories, 3M Co.
St. Paul, Minn. 55119

(Received February 21, 1969)

ABSTRACT

The adhesion properties of polymers are known to be influenced by both intermolecular forces operative at the interface and the rheological history of both bonding and unbonding. Recent adsorption and viscoelastic theories of adhesion and cohesion are implemented in a comprehensive examination of these phenomena. Eight peel force "master curves" extending over 14 decades of reduced rate and representing glassy state to flow region rheology are superimposed to provide a composite response envelope. Each master curve represents rate-temperature reduced adhesion of an alkyl acrylate adhesive (γ_c = 26 dyne/cm) to substrates ranging from low adhesion fluorinated polymers (γ_c = 15 to 17 dyne/cm) to polar polyamide surfaces (γ_c = 45 dyne/cm) and glass. The rate dependent transition from interfacial to cohesive failure, a subject not treated by adsorption theory, is shown to be coincident with the onset of entanglement slippage within the polymeric adhesive. Thermodynamic criteria of polymer adhesion are shown to be applicable only to the flow region of polymeric response. This study indicates that measured surface tensions or calculated surface energies of polymeric solids do not properly account for the contributions of three dimensional network structure of the polymeric bulk phase to its total work of cohesion. Evidence of true interfacial failure of a polymer-polymer bond is supported by critical surface tension measurements.

INTRODUCTION

THIS STUDY was undertaken to provide a comprehensive examination of new propositions emanating from recent "adsorption" [1-6] and "viscoelastic" [7-12] theory of adhesion. Adsorption theory involves consideration of surface and interfacial free energies and treats adhesion processes in terms of reversible thermodynamic equilibria. Viscoelastic theory, which is closely related to current concepts of polymer deformation and fracture [13, 14], treats adhesion phenomena as a rate process.

Adhesion measurements in peel provide a means of generating on a microscale a steady state unbonding process involving either interfacial or cohesive fracture. Peel adhesion data, by the use of a time-temperature reduced variable treatment [8-10], may be represented over a broad range of reduced

rate which normally spans 10 to 14 logarithmic decades. Inspection of such master curves of peel force versus reduced rate provides a new means of investigating the effects of both the interfacial thermodynamics and the rheology of the system.

One specific objective of this study was to examine the correlation of peeling force P with calculated values of work of adhesion [12], W_a, and spreading coefficient [6], $S = W_a - W_c$, for the solid-solid interfacial failure of dissimilar polymers. A second objective was to provide a further analysis [8, 10] of the rheological processes which control the rate and temperature dependent transition from interfacial to cohesive failure first reported by Bright [15]. Rate dependent adhesive to cohesive failure transitions are neither predicted nor treated by thermodynamic theories of adhesion [1-6].

ADHESIVE BULK PROPERTIES

A single amorphous and noncrosslinked alkyl acrylate copolymer adhesive was applied in tape bonds to seven polymeric surfaces of varying critical surface tension, γ_c, and to glass. This polymeric adhesive contained no additives such as low molecular weight tackifiers or inorganic pigments. Both surface and bulk properties were considered in the selection of this material.

This copolymer of 50:50 mole percent isoamyl acrylate:neopentyl acrylate, displayed a glass transition temperature $Tg = -43 \pm 1°C$, as measured by dilatometric [16] and refractive index techniques [17]. A number average molecular weight $M_n = 1.03 \cdot 10^6$ was determined by membrane osmometry using a toluene solvent. The adhesive displayed a density $\rho = 0.9402$ at 25°C. Thermal expansivities of $\alpha_G = 1.74 \cdot 10^{-4}\ °C^{-1}$ and $\alpha_L = 6.75 \cdot 10^{-4}\ °C^{-1}$ for the respective glass and liquid state were calculated by application of the classic Lorentz-Lorenz equation to the refractometric data.

Viscoelastic response was measured in terms of the tensional relaxation modulus $E(t)$ following the methods of Tobolsky [18] on an Instron equipped with a variable temperature air bath which controls to ± 0.1°C. The results, reduced by standard WLF superposition, are presented in Figure 1 as a master curve of shear relaxation modulus, $G(t)\ T_o/T = E(t)T_o/3T$ versus reduced reciprocal time (a_T/t) for a reference temperature $T = T_o = 296°K$. The time-temperature shift factor a_T is calculated by the following form of the WLF [19] expression:

$$\log a_T = 9.8 - \frac{17.44\,(T - T_g)}{51.6 + T - T_g} \tag{1}$$

which operates for $T_o = 296°K$ and $T_g = 230°K$.

Figure 1 represents relaxation data covering a time range from 3 to 3000 sec. and a temperature range from $(T_g - 7)°C$ to $(T_g + 93)°C$. The quality of superposition indicates that the standard reduced variables treatment ap-

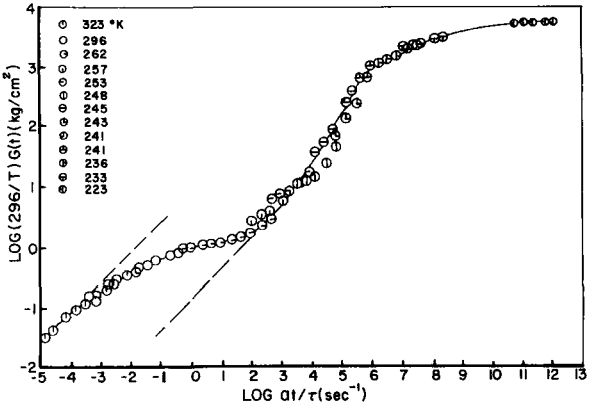

Figure 1. Shear relaxation modulus of an alkyl acrylate adhesive measured at 13 temperatures and reduced to 296°K.

plies to this polymer. Equivalently good results have been obtained by superposition of measured storage G' and loss G'' modulus data obtained for this copolymer but which are not reported here. The relaxation master curve displays the characteristic transitions from flow region to rubbery state plateau response followed by the rubber to glass transition region with increasing values of log a_T/t.

Several molecular parameters of interest may be estimated from the relaxation modulus master curve presented in Figure 1. The number average molecular weight between crosslinks M_e may be estimated, after the manner of Ferry [20], by application of the following equation from the kinetic theory of elasticity:

$$M_e = \frac{\rho RT}{G_e} \tag{2}$$

where ρ is polymer density, R the gas constant (84.7 Kg cm/deg. mole), T absolute temperature, and $G_e = 1.2$ Kg/cm^2 the relaxation modulus at the inflection point of the rubbery state plateau. A calculated value of $M_e = 21{,}000$ is obtained from equation (2).

By measuring Δ, the span of log a_T/t in the rubbery plateau region which separates the d log $(296G/T)/d$ log$(a_T/t) = 1/2$ regions (indicated by the dashed curves of Figure 1), the ratio $\overline{M}_n/2M_e$ may be calculated by either of two approximations. The first from Ferry [20] provides the following relation:

$$\Delta = 2.4 \log(\overline{M}_n/2M_e) \tag{3}$$

the second from Bueche [21] states:

$$\Delta = \log 4 + 4.5 \log(\overline{M}_n/2M_e) \tag{4}$$

From Figure 1 the value of Δ may be determined as $\Delta \simeq 3.4$ and from equation (3) the ratio $\overline{M}_n/2M_e = 26.4$ and $\overline{M}_n = 1.1 \cdot 10^6$. The second estimation by the Bueche equation (4) provides lower values of $\overline{M}_n/2M_e = 4.2$ and $\overline{M}_n = 1.77 \cdot 10^5$. It may be noted that the Ferry relation (3) provides a good agreement with $\overline{M}_n$ as measured by osmometry. As pointed out by Bueche [21] both equations (3) and (4) fail to fully account for the effect of entanglements on viscoelastic properties and therefore provide only rough estimates of the average number of entanglements per polymer chain as given by $\overline{M}_n/2M_e$.

SURFACE PROPERTIES

Adhesion studies were conducted on eight adherend surfaces which are listed in Table 1 in the order of decreasing critical surface tension γ_c. The glass surface indicated in Table 1 was obtained through use of clean microscopic slides on which water spreads indicating a $\gamma_c > 72.8$ to water. The polymeric materials listed in Table 1 are either amorphous glasses or semicrystalline over the temperature range (-35 to $+70$°C) of bonding or unbonding reported here. These adherends were prepared as smooth films and their chemical composition confirmed by infra-red adsorption analysis of the bulk polymer.

The critical surface tensions of these films were experimentally estimated using the sessile drop technique and measurement of the advancing contact angle after the method of Zisman [5]. Table 2 identifies the liquids utilized in the contact angle experiments. Measured values of liquid surface tension, obtained by the DuNouy ring method at 23 ± 0.5°C, are in reasonable agreement with published values as indicated in Table 2.

Table 3 reports the measured values of the cosine of the contact angle, $\cos \theta$, formed between liquid and polymer solid. In addition to the seven polymers listed in Table 1, measurements were conducted on the adhesive

Table 1. Substrate Surfaces

Number	Composition
1	glass
2	polycaprolactam (Nylon 6)
3	polystyrene
4	polytrichlorofluoroethylene (Kel-F)
5	polyvinylfluoride
6	polyvinylidene fluoride
7	polytetrafluoroethylene (Teflon TFE)
8	C_2F_4-C_3F_6 copolymer (Teflon FEP)

surface A and on the tape backing surface B, the latter surface produced by interfacially unbonding the coated adhesive at low temperature.

The starred data points of Table 3 were utilized in obtaining linear curves, see Figure 2, of cos θ vs. γ_L which, upon extrapolation to cos $\theta = 1.0$, provides an estimate of γ_c for the solid. The experimental values of γ_c for the nine polymeric surfaces are tabulated in Table 3.

The critical surface tension, $\gamma_c = 26$, of the adhesive surface A is typical of a nonpolar hydrocarbon surface and is intermediate between the characteristic Zisman [5] values $\gamma_c = 22$ to 24 for $-CH_3$ side groups and $\gamma_c = 31$ for $-CH_2-$ main chain elements. From this result it may be expected that

Table 2. Surface Tensions of Spreading Liquids

Liquid	Reference Value[23] of γ_L (20°C.)	Measured of γ_L (23°C.)
Water	72.8	72.8
Glycerol	63.4	67.3
Formamide	58.2	60.7
Methylene Iodide	50.8	52.9
Tetrabromoethane	49.7	51.9
α-Bromonaphthalene	44.6	45.6
Hexachlorobutadiene	36.0	39.4
Toluene	28.5	30.6

Table 3. Contact Angle Measurements and Estimation of Critical Surface Tension of Nine Polymer Surfaces

Substrate	A	B	2	3	4	5	6	7	8
γ_L					Cos θ				
72.8	—.208	.429	.208*	.070*	—.087*	.225*	—.052	—.484*	—.304*
67.3	—.375*	.381*	.122	.139*	—	.400*	—	—.342*	—.203*
60.7	—.139*	.603*	.559*	.242*	.139*	.616*	.438*	—.174*	—.044*
52.9	—.035*	.781*	.755*	.799†	.491*	.669*	.453*	.122*	.075*
51.9	.407†*	.988*	.899*	.961†	.545*	.958*	—	.052*	.329
45.6	.308†*	1.0	.974*	.961†	.899	.990*	.921	.156*	.264*
39.4	.358†*	1.0	.996	.961†	.940	.985	.985	.308*	.480
30.6	.951†*	1.0	.998	.993†	.998	—	.961*	.588*	.681*
Experi. γ_c dyne/cm	26	49	45	33	37	44	30	15	17
Pub. (5, 22) γ_c dyne/cm	—	—	42	33	31	28	25	18.5	—

* indicates data points utilized in the graphical estimation of γ_c.
† detectable solvent type erosion of substrate surface by liquid.

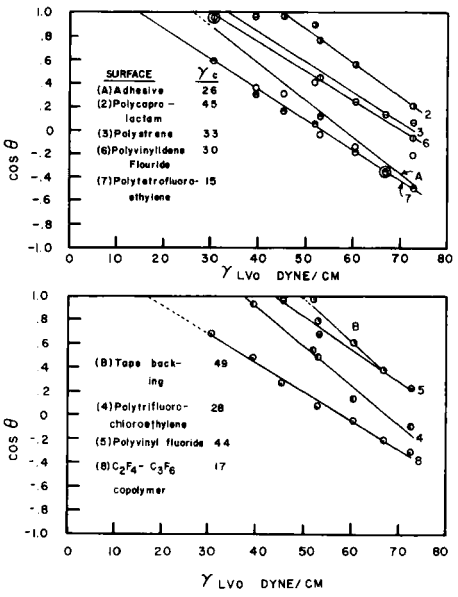

Figure 2. Wettability of various liquids on nine polymeric substrates.

the adhesive contributes only dispersion forces to an interfacial interaction.

The interior surface of the polyethyleneterephthalate backing *B* displays a high critical surface tension $\gamma_c = 49$. This result is in reasonable agreement with the published value $\gamma_c = 43$ for this polymer [5] and indicates that appropriate mechanical desorption of the solvent coated adhesive regenerates the higher energy surface of the polyester film. The conditions of this interfacial separation within the tape will be displayed in later data and discussion.

With the exception of polyvinyl fluoride the experimental and reference values for γ_c for the seven polymeric substrates listed in Table 1 and Table 3 agree within 6 dynes/cm. The extraordinary high value $\gamma_c = 44$ dyne/cm obtained for polyvinyl fluoride is not due to a major defect in the data of Table 3 but rather to the emphasis placed in the extrapolation of Figure 2 upon interactions of polar and hydrogen bonding liquids. A similar value of $\gamma_c = 40 \pm 3$ dyne/cm is obtained from the data of Ellison and Zisman [24] for polyvinyl fluoride if the linear extrapolation to $\cos \theta = 1.0$ is based exclusively upon liquids with $\gamma_L \geq 44$ dyne/cm. The greatest scatter of data, as indicated in Figure 2, was associated with the adhesive surface *A*. For this latter curve all data could be incorporated in a rectilinear band having $\gamma_c = 26 \pm 6$ dyne/cm.

A portion of the liquid-solid interactions, indicated by daggers in Table 3, gave evidence of surface erosion of the solid film. These effects were noticeable on the adhesive surface *A* and polystyrene surface. This phenomena

indicates the liquid had partially dissolved the polymer surface.

The surfaces indicated in Table 1 through Table 3 present a considerable range of critical surface tension γ_c. The critical surface tension of a low energy solid is now considered to be a first approximation measure of surface free energy [1-6]. Good and Girifalco [1-3] propose the following relation for interfacial tension γ_{SL} between a liquid and solid:

$$\gamma_{SL} = \gamma_S + \gamma_L - 2\phi(\gamma_S\gamma_L)^{.5} \tag{5}$$

where γ_S and γ_L are the respective solid and liquid surface free energy and ϕ a correction factor now defined [3] in terms of molecular geometries and forces of interaction of the adjacent phases. Fowkes [4] has provided a relation of similar character:

$$\gamma_{SL} = \gamma_S + \gamma_L - 2(\gamma_S^d\gamma_L^d)^{.5} \tag{6}$$

where γ_S^d and γ_L^d refer to the dispersion force contribution to solid and liquid surface free energy. In the proposition of Fowkes, if one of the adjacent phases contributes only a dispersion force interaction then the second adjacent phase is similarly restricted to dispersion force contributions.

In this discussion we will consider the acrylic adhesive to act as the liquid phase of pure dispersion force character such that $\gamma_c = \gamma_L = \gamma_L^d = 26$ dyne/cm. The polymeric adherends included in this study will also be considered to display surface properties of a dominantly dispersion force character such that $\gamma_C = \gamma_S = \gamma_S^d$. From these simplifying considerations equation (6) may be rewritten as:

$$\gamma_{LS} = \gamma_L + \gamma_S - 2(\gamma_L\gamma_S)^{.5} \tag{7}$$

where γ_c now represents the apparent surface free energy of the polymeric adherend. The statement of equation (7) is equivalent to setting $\phi = 1.0$ in equation (5).

The reversible work of adhesion W_a is given by the following standard expression:

$$W_a = \gamma_L + \gamma_S - \gamma_{LS} \tag{8}$$

By combination of equation (7) and (8) we obtain:

$$W_a = 2(\gamma_L\gamma_S)^{.5} \tag{9}$$

The work of cohesion for the liquid is simply:

$$W_c = 2\gamma_L \tag{10}$$

The spreading coefficient $S = W_a - W_c$ of the liquid on the solid is, from equations (9) and (10), given by

$$S = 2[(\gamma_L\gamma_S)^{.5} - \gamma_L] \tag{11}$$

Using the experimental values of γ_c for the polymer adherends as represent-

ing γ_S and for the adhesive $\gamma_L = \gamma_c = 26$ dynes/cm we may calculate first approximation values of W_a, W_a^2, and S for the eight interfaces identified in Table 3.

The results of this calculation are presented in Table 4. By use of the simplifying assumptions leading to equations (9) through (11) we present in Table 4 a maximum estimate of W_a and S values. The real values particularly for polar substrates such as glass (A-1) and polycaprolactam (A-2) may be less due to failure to subtract the noninteracting polar forces [4]. The second important source of error, the assumption of complete wetting of the microscopically rough adhesive-adherend surfaces, is given special attention in the following section.

From adsorption theory a prediction that logically follows from Table 4 is that all bonds, except A-7 and A-8, should display cohesive failure if an equilibrium wetting is achieved between adhesive and adherend. This prediction follows from the fact that the calculated spreading coefficient is positive and the interfacial work of adhesion exceeds the work of cohesion of the alkyl acrylate adhesive. In the eventuality of interfacial failure the further prediction of Table 4 is that bond strength, which may correlate to W_a or W_a^2, should decrease monotonically with γ_S of the adherend [12]. Previous studies of a less extensive character have indicated that neither of these simple predictions of adsorption theory are strictly followed in polymeric unbonding processes [10, 12, 15]. The following sections provide some further clarification of these issues.

RHEOLOGY OF BONDING

The test tape of the following properties and geometry:

$$E = 3.45 \cdot 10^4 \frac{\text{Kg}}{\text{cm}^2} = \text{Young's modulus of flexible member (23°C)}$$

Table 4. Maximum Estimates of Interfacial Adhesion Properties

Interface	γ_S	W_a (erg/cm^2)	W_a^2 (erg^2/cm^4)	$S = W_a - W_c$ (erg/cm^2)
A-1	>72.8	>87.0	>7570	>35.0
A-B	49	71.4	5100	19.4
A-2	45	68.4	4680	16.4
A-3	33	58.2	3390	6.2
A-4	37	66.2	3870	10.2
A-5	44	67.4	4550	15.4
A-6	30	56.0	3140	4.0
A-7	15	39.8	1580	−12.2
A-8	17	41.8	1750	−10.2

$h = 1.27 \cdot 10^{-3}$ cm = half thickness of flexible member
$a = 2.29 \cdot 10^{-3}$ = thickness of adhesive layer
$b = 1.27$ cm = bond width

was mechanically laminated to the substrate surface using six passes of a 1.25 cm. diameter stainless steel roller loaded to 1.5 Kgm. This mechanized bonding procedure eliminates visible areas of entrapped air at the adhesive-adherend interface. This mechanical lamination is followed by a thermal conditioning of the bond under no applied force for 60 minutes at 70°C. From the propositions of the reduced variables presented in equation (1) this reasonable dwell time at 70°C. is equivalent to an extended bonding time at 23°C.

Applying equation (1) we may calculate the reduced bonding time t_{T_0} at 23°C. as:

$$t_o = t/a_T = 3.6 \cdot 10^3 (2.0 \cdot 10^2) = 7.2 \cdot 10^5 \text{ sec.}$$

This extended reduced bonding time may be referred to the polymer viscoelastic response illustrated in Figure 1 for a reduced reciprocal time log $a_T/t = -5.86$ which is characteristic of flow region response. This region of long time is several logarithmic decades to the left of that region indicated in Figure 1 where entanglement restraints would prevent free segmental diffusion of the acrylic copolymer to the adherend interface. We may assume, and the peel adhesion data indicate, that the adhesive-adherend bond has achieved an essential equilibrium of diffusional processes under this bonding condition.

This fundamental point concerning the kinetics and equilibrium conditions of polymer bonding is discussed at greater length elsewhere [11]. One important prediction of this viscoelastic criteria of bonding is that when $t_o >> \tau_m$, where τ_m is the terminal relaxation time of the adhesive, segmental interdiffusion should occur at the interface formed by the adhesive bonded to itself. Tests of this prediction for $t_o = 7.2 \cdot 10^5$ sec. indicated the autoadherend interface of the acrylic copolymer adhesive was equivalent in strength and indistinguishable from the bulk polymer.

PEEL ADHESION

Peel adhesion measurements were conducted at a peel angle $\omega = 180$ degrees $= \pi$ rad. using controlled rates ranging from 50 cm/min. to 0.025 cm/min. Tests were conducted on an Instron tensile tester in a temperature control chamber regulated to provide a variation of less than 0.1°C. A portion of the bonds involving flexible adherends were tested on a rotating drum tester which has previously been described [25]. The remainder of the bonds were affixed to glass plates by means of a double coated tape bond between the adherend and glass surface. The results between the two methods of

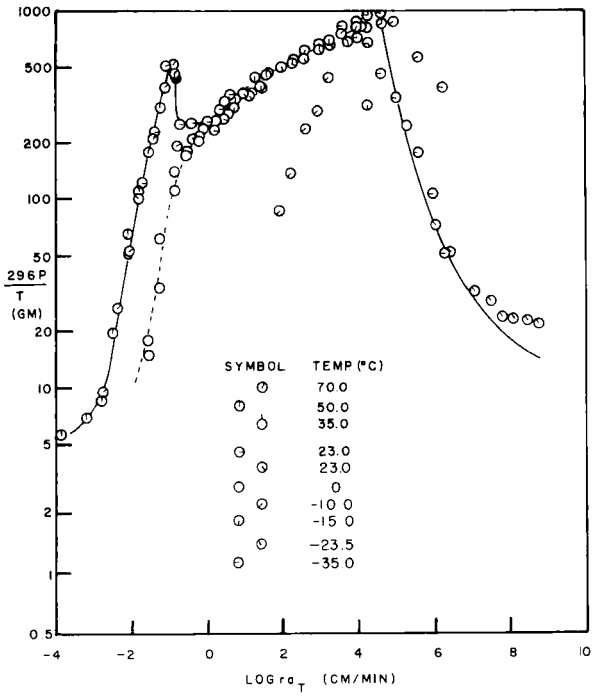

Figure 3. Temperature reduced peel adhesion to glass.

testing were indistinguishable. Tests were conducted at seven to eleven temperatures ranging from 70°C. to —35°C. and at nine or more rates at each temperature. At least one bonding procedure was required for each temperature of test so that each master curve of peel force versus reduced rate reflects the bonding reproducibility.

The measured peel force P is reduced by the standard convention [10] to a reduced peel force PT_o/T and the peel rate r to a reduced rate ra_T where $T_o = 296°K$ and a_T is defined by equation (1). The reduction applied to the peel data is exactly equivalent to that already described with regard to adhesive bulk properties. The reduced data are presented on bilogarithmic scales of reduced peel force P $296/T$ and reduced rate ra_T due to the broad ranges of each variable. The results of peel adhesion measurement are displayed in Figure 3 through Figure 10. These illustrations follow the sequence of Table 1 in order to illustrate the effect of decreasing critical surface tension of the adherend. These master curves display nonselected data and therefore represent a full record of the result.

As shown in Figures 3 through 10 a high proportion of the data superimpose very well on the peel adhesion master curves. The scattering of data points from the master curve is most evident in negative slope regions where

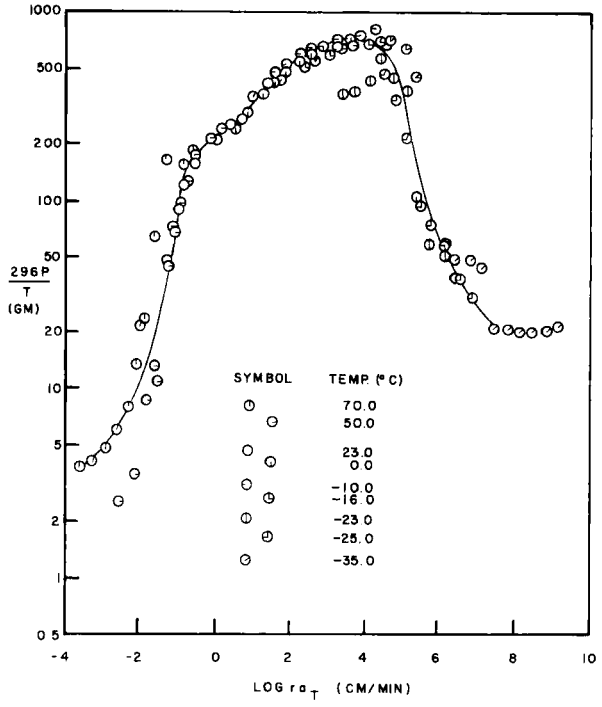

Figure 4. Temperature reduced peel adhesion to polycaprolactam (Nylon 6).

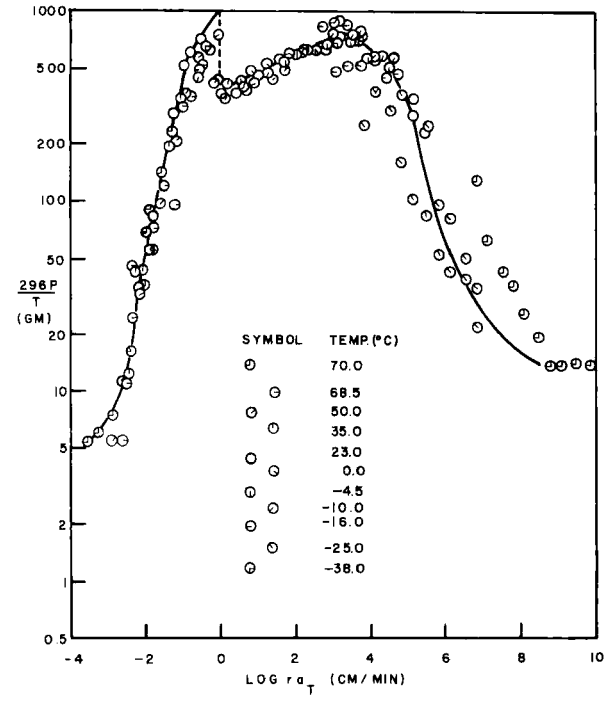

Figure 5. Temperature reduced peel adhesion to polystyrene.

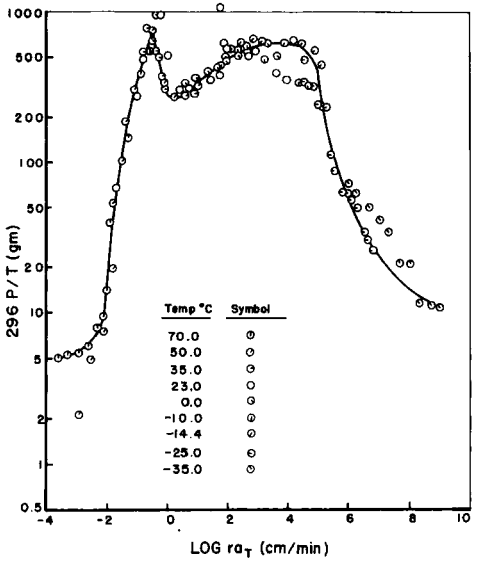

Figure 6. Temperature reduced peel adhesion to polytrifluorochloroethylene (Kel-F).

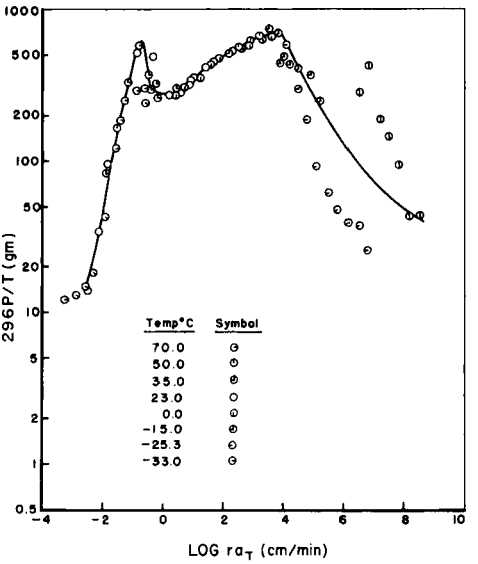

Figure 7. Temperature reduced peel adhesion to polyvinyl fluoride.

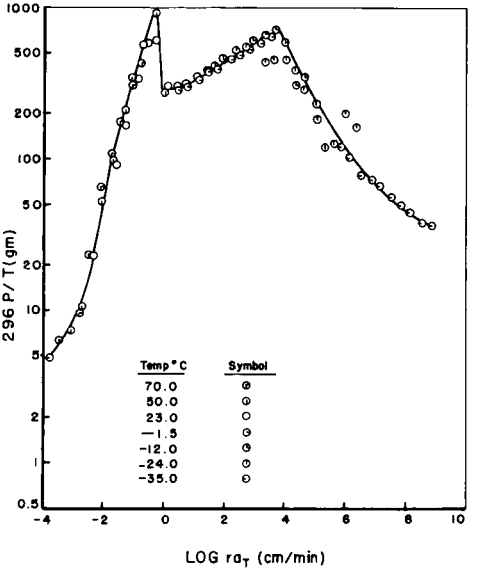

Figure 8. Temperature reduced peel adhesion to polyvinylidene fluoride.

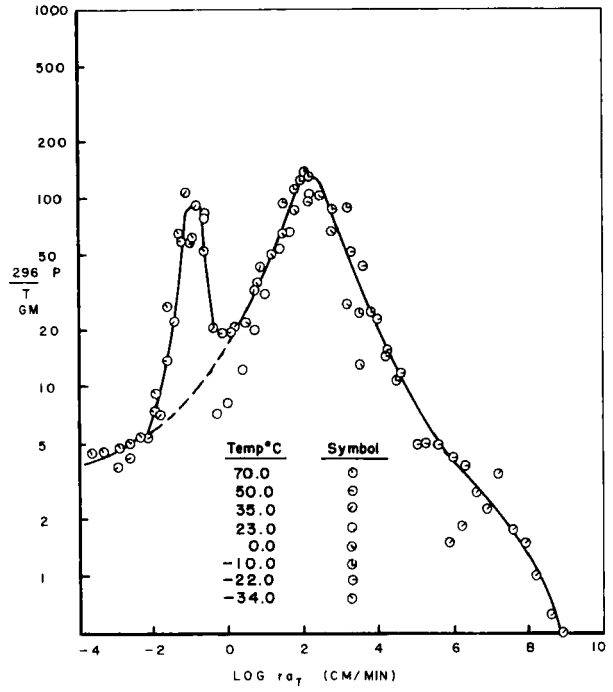

Figure 9. Temperature reduced peel adhesion to polytetrafluoroethylene (Teflon TFE).

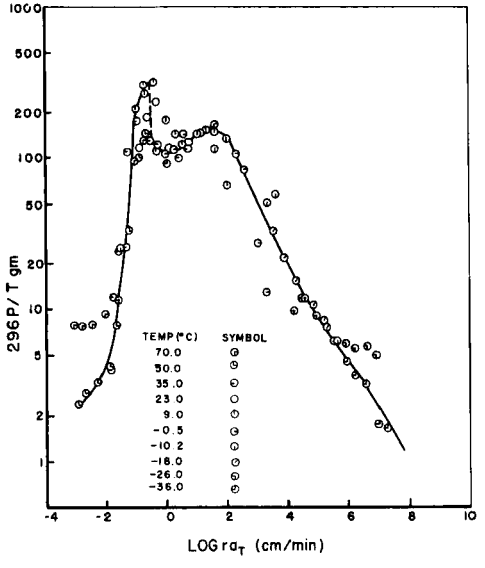

Figure 10. Temperature reduced peel adhesion to a tetrafluoroethylene-hexafluoropropylene copolymer (Teflon FEP).

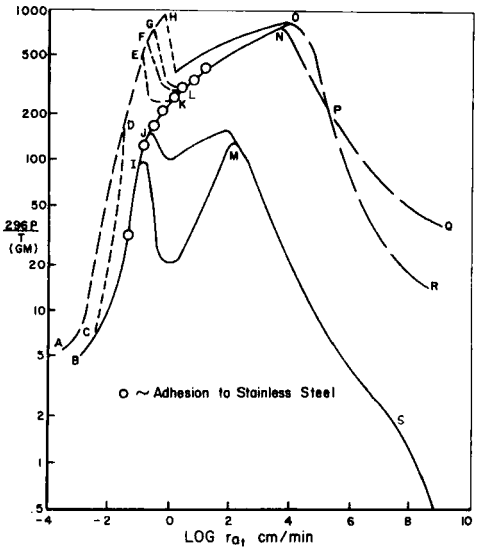

Figure 11. Composite response envelope of temperature reduced peel adhesion to eight substrate surfaces (see Table V for adherends and unbonding mechanisms).

the master curve displays a reduction in peel force P 296/T with increased rate ra_T. These negative slope regions of peel response are associated with slip-stick stripping action related to a rate instability of peel force which is a secondary property of the primary force-rate function [10]. Rather than discuss the individual features of each master curve, all master curves of Figure 3 through Figure 10 may be organized into the composite response envelope presented in Figure 11. The terminal and junction points of the curve segments of Figure 11 have been letter coded. The P vs. ra_T master curve for each adherend may be described by the simplest connection of the letter code points tabulated in Table 5. This table also describes the curve segments in terms of unbonding mechanisms.

Figure 11 presents the family of master curves representing the peel adhesion properties of the test tape to all eight adherend surfaces. In Figure 11 additional information is presented concerning the mechanism of unbonding. A significant feature of Figure 11 is the evident strong correlation between master curves for dissimilar adherends. Also evident in Figure 11 are the multiple transitions of unbonding mechanism which appear to be dominantly functions of reduced rate rather than adhesive-adherend combination.

It should be recalled that a single function of a_T, as given by equation (1), is applied to the superposition of all peel data to the reference temperature $T_0 = 296°K$. It is quite evident from the illustrations of Figure 3 through

Figure 11 that the apparent activation energy of unbonding:

$$\Delta H_a = 2.303\ R\ \frac{d\ \log\ a_T}{d(1/T)} \tag{12}$$

is independent of both the surface chemistry of the adherend and the mechanism of unbonding (interfacial or cohesive failure). The successful application of the WLF [19] equation to both the viscoelastic and peel adhesion data indicates that temperature influences these properties only indirectly by its effect upon the fractional free volume of the polyacrylate adhesive. This fundamental connection between adhesion and rheological phenomena has been made previously [8-11] and is reconfirmed in these extensive data.

INTERFACIAL UNBONDING

In order to establish that interfacial failure, as identified in the master curves of Figure 11 and in Table 5, was being realized a special experiment was undertaken. Confirmation of interfacial failure may be obtained by conducting contact angle measurements on a fresh adherend surface and comparing these results with a surface subjected to a bonding and peeling cycle. Polycaprolactam, $\gamma_c = 45$ and polytetrafluoroethylene, $\gamma_c = 15$ were most suitable for this experiment since their γ_c values differed most substantially from that of the adhesive. The data presented in Figure 12 show the comparative wettability of these adherends before and after tape bonding for 60 min. at 70°C. and peeling at 50 cm/min. at 23°C. As the results indicate

Table 5. Adherend and Unbonding Mechanism As Identified In the Composite Master Curves of Figure 11

Adherend	*Letter Code Points*
Glass	ADFLNOPR
Nylon 6	BCKNOPR
Polystyrene	ADEHOPR
Kel-F	BCDGLNOPR
Polyvinylfluoride	ADFLNPQ
Polyvinylidene fluoride	ADGLNPQ
Teflon TFE	BCIMS
Teflon FEP	BCJMS

Curve Type	*Boundary Stress*	*Mechanism of Unbonding*
(1) Solid	σ_1	Interfacial adhesive from adherend
(2) Long Dash	σ_2	Interfacial adhesive from tape backing
(3) Medium Dash	σ_3	Cohesive within the adhesive bulk
(4) Short Dash		Transition between above mechanisms

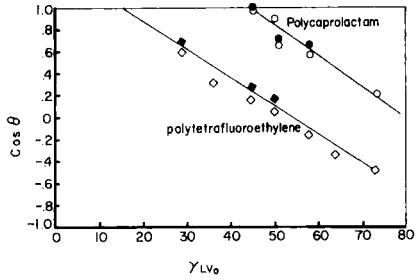

Figure 12. Wettability of various liquids on two polymeric substrates. Open symbols designate fresh substrate surface; closed symbols designate surfaces subsequent to tape bonding for 60 min. at 70°C. and peeling at 50 cm/min. at 23°C.

the bonding and peeling did not appreciably alter the surface properties of the two adherends. If even a monolayer of polymeric adhesive had remained at the adherend surface the solid data points of Figure 13 should form a third curve characteristic of $\gamma_c = 26$ for the polyacrylate adhesive.

A previous definition [10] of interfacial unbonding stipulates that the process should occur substantially at the adhesive-adherend interface and be influenced by both:

a. The perfection of the interfacial bond
b. The surface chemistry and physics of the adherend

In this study the contact angle data of Figure 12 establishes the location of the failure plane at the interface. The singularity of peel adhesion properties for each case of interfacial failure reported in Figure 3 through Figure 11 is a further indication of the measured interfacial response. As shown in Figure 11, all bonds failing by a cohesive mechanism exhibit equivalent bond strengths in peel.

DISCUSSION

The time scales of the stress relaxation data of Figure 1 and the peel adhesion data of Figure 3 through Figure 11 may be related by the following expression from peel theory [8, 9, 10]:

$$\frac{1}{t} = \frac{2\pi r}{\lambda} \tag{13}$$

where t is relaxation time, r is peel rate and λ is the wave length of the sinusoidal cleavage stresses in peel. Separate experiments using a new instrument called a "bond stress analyzer" [26] permitted a direct measurement of λ for the tape of this study during unbonding from a stainless steel adherend at 23°C. and a peel angle $\omega = 180$ degrees. The rate and peel forces measured in this experiment are indicated in Figure 11. These experiments provided a nearly constant value of $\lambda = 0.06 \pm .10$ cm over the range of rates studied. Peel adhesion theory predicts that $\lambda \propto G^{-1/4}$ where G is the adhesive shear modulus and is therefore reasonably insensitive to rate or

relaxation time changes. Applying this measured value of λ to equation (13) we obtain the appropriate proportionality relation between the reciprocal time scales of Figure 1 and Figure 11:

$$a_T/t\ (\text{sec.}^{-1}) = 1.75 \left[\frac{\text{min.}}{\text{cm. sec.}} \right] r \left[\frac{\text{cm.}}{\text{min.}} \right]$$

In other words, a peel rate of $ra_T = 0.57$ cm./min. in Figure 11 corresponds to a reciprocal time in Figure 1 of $1/ta_T = 1.0\ \text{sec}^{-1}$. It follows that the time scales of Figure 1 and Figure 11 are related by:

$$\log\ a_T/t = \log\ ra_T + .243 \tag{14}$$

over the presented times and rates. The important consequence of this direct time-rate relation lies in the correlations which may be drawn between the viscoelastic state and the adhesion properties of the alkyl acrylate adhesive.

Previous analysis of peel-adhesion has shown that peel force P is maximized in regions of maximum viscoelastic dispersion [8, 9, 10]. This relationship is identified in the following equation of peel force measured at a peel angle of 180 degrees:

$$P = \frac{ba}{12} \frac{\sigma^2}{G} \tag{15}$$

Equation (15) states that P is directly proportional to the internal work of deformation of the adhesive as expressed by the ratio $(\sigma^2/2G)$. Both the boundary tensile stress σ and shear modulus G of equation (15) are time dependent quantities. The σ parameter of equation (15) is a true adhesion property of the bond by the fact that it is related to the mechanism of unbonding. The unbonding process follows a least work mechanism and in the example of this study may display a σ_1, σ_2, or σ_3 where the subscript numbers identify the numbered failure mechanisms reported in Table 5. The shear modulus G of equation (15) is a true rheological parameter since it reflects only adhesive bulk properties independent of the unbonding mechanism.

It is now known from recent experimental studies of the internal cleavage stresses in peel that the σ calculated by use of equation (15) is an idealization not realized in the actual experiment due to complex cavitation and adhesive filamentation [25]. For peeling conducted at a peel angle of 180 degrees a direct correlation has been shown to exist between peel force and measured unbonding stresses which are directly relatable to the idealized stress described by equation (15).

With this understanding that σ represents an idealization relatable to real phenomena we rewrite equation (15) in the following form:

$$\sigma(ra_T) = \left[\frac{12}{ba} P(ra_T)\ G(ra_T) \right]^{1/2} \tag{16}$$

Equations (14) and (16) permit calculation of the rate functions of $\sigma(ra_T)$ based on measured rate functions of peel force $P(ra_T)$ and shear modulus $G(ra_T)$. The constants $b = 1.27$ cm. and $a = 0.00299$ cm. of equation (16) are respectively bond width and adhesive thickness. The reduced rate dependence of the calculated boundary stress functions for four representative adherends are presented in Figure 13.

In general agreement with present theory of polymer cohesion [13, 14] and viscoelastic theory of peel adhesion [8, 9, 10] these σ functions shown in Figure 13 increase or plateau with increased values of ra_T or a_T/t. In other words, the maxima and minima in the peel force versus rate functions for all interfaces, as summarized in Figure 11, apparently result from the curious interplay of monotonically increasing functions of σ and G as they interact in the ratio $\sigma^2/2G$ which describes the work of adhesive deformation. The single exception to the above observation is displayed in the σ versus ra_T curve for Teflon TFE where log $ra_T = 1.0$ to 0.

A particularly striking property of the calculated σ functions is shown in the curve for the polystyrene adherend illustrated in Figure 13. This bond displays two changes in mechanism of failure so that the complete curve involves branches of σ_1, σ_2, and σ_3 functions as identified by the curve code and mechanism numbers of Table 5. These three σ_1, σ_2, and σ_3 branches are apparently smoothly intersecting functions as indicated by the continuous nature of the master curve of σ over the full range of reduced rates.

The boundary stress function for Nylon 6 displays a remarkably smooth

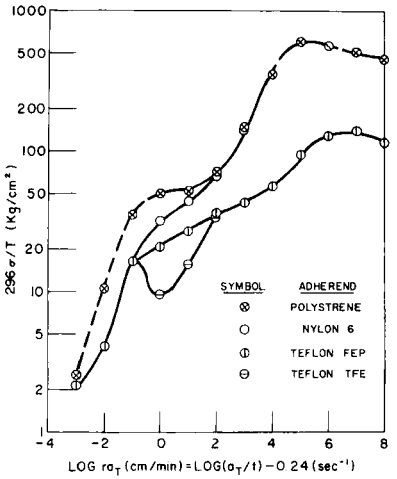

Figure 13. Temperature reduced boundary cleavage stress for four polymeric substrates (see Table V for unbonding mechanisms).

transition from the low adhesion response of the fluorinated surfaces to the high adhesion response of the polystyrene surface with increased peel rate as shown in Figure 13. An explanation of this phenomena is not available except through some consideration of the fact that the Nylon 6 surface is polar in character. Patterson [27] has shown that a polyamide surface interacts more strongly with hydrogen bonding than with non-hydrogen bonding liquids. The alkyl acrylate adhesive of this study is considered to be nonpolar and the interaction with Nylon 6 is expected to be primarily through dispersion force interactions. As indicated in Figure 11 and Figure 13 the tape to Nylon 6 bond is subject to only interfacial failure involving the σ_1 mechanism at low rates and the σ_2 mechanism at high rates where log $ra_T \geq 5.0$. It is interesting to note that the peel force to Nylon 6 is equivalent to stainless steel at intermediate rates as indicated in Figure 11. The hydrated oxide surface of steel would also be expected to interact with liquids in much the same manner as that indicated by Patterson for polyamides.

The boundary stress curves for the fluorinated surfaces display lower σ values over the full range of ra_T displayed in Figure 13 and failure by the σ_1 mechanism as predicted by the calculations tabulated in Table 4. The further prediction of Table 4, that cohesive failure should result for all other adherend surfaces is fulfilled, with the exception of Nylon 6, at rates where log $ra_T \leq 0$. At these low rates all cohesive failures follow the σ_3 function displayed in Figure 13 for polystyrene. As previously indicated by Bright [15], true cohesive fracture reflects bond strengths which are independent of the adhesive-adherend interfacial properties.

The reasons for the transitions from cohesive σ_3 to interfacial σ_1 type failure of surfaces displaying values of $S \geq 0$ in Table 4 when peel rates are increased above log $ra_T \geq 0$ are evident from a consideration from polymer physics. It may be recalled that bonding was accomplished under a condition which has been indicated to provide an equilibrium interfacial adsorption. At high unbonding rates the interfacial unbonding from all adherends indicates that interfacial interdiffusion of polymer segments was not an unintentional further step in this bonding process. It should be further recognized that any hypothetical failure plane through the adhesive bulk would exhibit substantial interdiffused polymer chains which provide a contribution to the work of cohesion not measured by the critical surface tension of the adhesive free surface. Furthermore at high values of log ra_T or log a_T/t these chain segments are restrained from moving by the entanglement network characterized in an earlier section.

At low reduced rates of peel or low values of reduced reciprocal time the rate of entanglement slippage exceeds the rate of adhesive deformation as indicated by the onset of the terminal zone of viscoelastic response shown in Figure 1 where log $a_T/t < 0$. The transition from interfacial to cohesive

fracture in the manner predicted by Table 4 is thus associated with the removal of the same restrictions of molecular motion in the adhesive which are operational in the equilibrium bonding process. The higher peel forces shown in Figure 11 and boundary stresses shown in Figure 13 for the cohesive fracture mechanism reflect this additional work of disentanglement of the polymer network. It may be noted in both Figure 11 and Figure 13 that this added work of disentanglement characteristic of cohesive fracture diminishes rapidly with decreased rate such that P and σ values for cohesive and interfacial failure are nearly equivalent at log $ra_T \simeq -3.0$.

This discussion has attempted to illustrate the close connection between peel adhesion properties and adhesive viscoelasticity that is evident by superimposing the rate and reciprocal time scales of Figure 11 and Figure 1 through use of equations (13) and (14). The complex phenomena of peel adhesion summarized in Figure 11 are partially interpretable in terms of both rheology and interfacial thermodynamics.

Calculation of the idealized boundary stress functions illustrated in Figure 13 indicate that the critical fracture stresses for both interfacial and cohesive unbonding are complex functions of rate or time which are not yet fully understood. Works of adhesion W_a and cohesion W_c obviously enter into the magnitude of the calculated σ values but close correlation of these parameters is not evident.

The operation of purely thermodynamic criteria of adhesion and cohesion appear most successful when no restraints on molecular motion of the polymeric adhesive are operative. This condition is realized only in the flow region of response. If the adhesive exhibits substantial elastic restraints on molecular motion proper consideration is demanded concerning the influence of these restraints on both bonding and unbonding phenomena. This restriction on thermodynamics is imposed primarily by the fact that the adjacent polymeric phases possess a three dimensional molecular structure not accounted for in surface energy measurements.

SUMMARY AND CONCLUSIONS

This study and pursuant analysis of data permit several general summary statements for the bond system reported on here:

1. Maximum peel adhesion in either interfacial or cohesive failure is associated with transition regions of viscoelastic response of the adhesive such as the glass-rubbery state transition and the rubbery state-flow state transition.
2. The apparent activation energy of unbonding, for both interfacial and cohesive failure, is defined by the WLF equation and is directly related to the fractional free volume state of the adhesive.

3. Correlation of peel adhesion properties to calculated works of adhesion and cohesion obtained by surface free energy measurement is confined to the flow (or terminal relaxation) region of adhesive rheological response.
4. Transitions from interfacial to cohesive failure are, in all examples studied, associated with the coincidence of the entanglement slippage rates with the rate of adhesive deformation. This rate condition identifies the rubbery state-flow state transition.
5. True interfacial failure is recognized for bonds which from surface energy criteria would be predicted to experience only cohesive failure. This common phenomena is associated with the fact that surface energy measurement does not account for the rate dependent work of disentanglement which is an important contribution to the work of cohesion of all high polymers at high rates of deformation or at low temperatures.

These conclusions are supported by both this study and earlier work [8-11]. These conclusions are considered generally applicable to any amorphous, linear, high molecular weight, polymer adhesive which forms an equilibrium adsorption interface (no interdiffusion) and which involves dispersion force interactions.

This discussion has not detailed the interesting and important micromechanisms of unbonding in peel which are now a subject of special study [26]. This method of investigation has been applied to the bond system reported here and will be the subject of a separate report [28].

ACKNOWLEDGMENT

The writer wishes to gratefully acknowledge the contribution of Mr. M. R. Hallwachs in determining molecular properties and Messrs. R. L. Huberty and R. S. Reylek in rheological and adhesion measurements.

REFERENCES

1. L. A. Girifalco and R. J. Good, *J. Phys. Chem., 61,* (1957), p. 904.
2. R. J. Good and L. A. Girifalco, *Ibid., 64,* (1960), p. 561.
3. R. J. Good, *Contact Angle Wettability and Adhesion,* 74, Adv. in Chem. Series, No. 43, A.C.S., Washington, D. C. (1964).
4. F. M. Fowkes, Ibid., 99.
5. W. A. Zisman, Ibid., 1.
6. L. H. Sharpe and Schonborn, Ibid., 189.
7. M. R. Hatfield and G. B. Rathmann, J. Phys. Chem., *60,* (1956), p. 957.
8. D. H. Kaelble, *Adhesives Age, 3,* No. 5, (1960), p. 37.
9. D. H. Kaelble, *Adhesion and Cohesion,* Ed: P. Weiss, 101 Elsevier Pub. Co., N. Y. (1962).
10. D. H. Kaelble, *J. Coll. Sci., 19,* (1964), p. 413.
11. D. H. Kaelble, *Treatise on Adhesion and Adhesives,* Chap. 6, Ed.: R. L. Patrick, Marcel Decker, Inc., N. Y. (1967).

12. C. A. Dahlquist, *ASTM Spec. Tech. Pub. No. 360,* 46, Amer. Soc. of Testing and Materials, Phil. (1964).
13. R. F. Landel and R. F. Fedors, *Fracture Processes in Polymer Solids,* Ed: B. Rosen, 361, Interscience Publishers, N. Y. (1964).
14. F. Bueche and J. C. Halpin, *J. Appl. Phys., 35,* (1964), p. 36.
15. W. M. Bright, *Adhesion and Adhesives,* Eds.: J. Clark, J. E. Rutzler, and R. L. Savage, 130, John Wiley and Sons, N. Y. (1954).
16. N. Bekkedahl, *J. Res. N.B.S., 42,* (1949), p. 145.
17. R. H. Wiley, G. M. Brauer, and A. R. Bennett, *J. Poly. Sci. 5,* (1950), p. 609.
18. A. V. Tobolsky, *Properties and Structure of Polymers,* John Wiley and Sons, N. Y. (1960).
19. M. L. Williams, R. F. Landel, and J. D. Ferry, *J. Amer. Chem. Soc., 77,* (1955), p. 3701.
20. J. D. Ferry, *Viscoelastic Properties of Polymers,* John Wiley and Sons, N. Y. (1961).
21. F. Bueche, *Physical Properties of Polymers,* Interscience, N. Y. (1962).
22. T. Fort, *Contact Angle Wettability and Adhesion,* 302, Adv. in Chem. Series No. 43, A.C.S., Washington, D. C. (1964).
23. W. A. Zisman, *Adhesion and Cohesion,* Ed. P. Weiss, 199, Elsevier, N. Y. (1962).
24. A. H. Ellison, and W. A. Zisman, *J. Phys. Chem., 58,* (1954), p. 260.
25. D. H. Kaelble, *Trans. Soc. Rheology, 3,* (1959), p. 161.
26. D. H. Kaelble, "Peel Adhesion: Micro-Fracture Mechanics of Interfacial Unbonding of Polymers, *Trans. Soc. Rheol., 9:2,* (1965), p. 135.
27. H. G. Patterson, *ASTM Spec. Tech. Pub. No. 360,* 32, Amer. Soc. of Testing and Materials, Philadelphia (1964).
28. D. H. Kaelble and R. S. Reylek, "Peel Adhesion: Rate Dependence of Micro Fracture Processes, *J. Adhesion,* Vol. 1, (1969), p. 124.